Synthesis of Angstrom-Scale Anatase Titania Atomic Wires

Chenmin Liu and Shihe Yang*

Department of Chemistry, William Mong Institute of Nano Science and Technology, The Hong Kong University of Science and Technology, Clear Water Bay, Kowloon, Hong Kong, China

ARTICLE

ABSTRACT Using a nonhydrolytic solution approach, we demonstrate the bulk synthesis of extremely thin crystalline TiO_2 atomic wires in the anatase phase with diameters reaching the atomic limit of a few angstroms (~4−5 Å). These nearly monodisperse, atomically thin, and soluble TiO_2 wires fill a most important size gap in nanowire fabrication. Preliminary results on photocatalytic activity of the atomic wires are also presented on degradation of methylene blue under visible light. These atomic wires are expected to promote exchanges between theory and experiments in fundamental studies of a one-dimensional (1D) system and provide unique building blocks to construct high-performance devices.

KEYWORDS: titania · anatase · atomic wires · nonhydrolytic synthesis · photocatalysis

Nowadays, nanowires with high aspect ratios can be routinely fabricated by a wide array of techniques.[1−3] From a synthetic point of view, a provoking question can be simply put: how thin can nanowires be made such that they are stable and useful in real-world settings? By using a simple nonhydrolytic solution approach, we have achieved bulk synthesis of anatase titania atomic wires with uniform diameters of approximately ~4−5 Å, which are as thin as about two to three Ti−O bonds across. The synthesis was realized by exercising control over the formation of a titanium-containing precursor from the reactions of titanium alkoxide and the subsequent growth of the TiO_2 atomic wires with the assistance of surfactants.

Not many materials can match the multipronged functionalities of titanium dioxide (TiO_2) yet have the virtues of low cost and environmental benignity. Traditional use of titania includes white pigment, corrosion-protective coatings, *etc.*[4,5] In 1972, Fujishima and Honda discovered the photocatalytic splitting of water on a TiO_2 electrode under ultraviolet light.[6] Since then, enormous efforts have been devoted to research on TiO_2 materials.[7] In the last two decades, work on the nanoscale has spectacularly expanded and augmented the utility of titania in heterogeneous catalysis, photocatalysis (water purification, air cleaning, and water splitting for the production of hydrogen), solar cells, and batteries, to name but a few applications.[8−11] Such applications were made possible by simply shrinking the physical dimensions of titania to the nanoscale regime where quantum size effect, small size effect, surface effect, and confinement effect become critical and new properties emerge. Another enabling strategy has been to dope titania nanostructures and thus modify their electronic and optical properties. Such doping significantly shifts the sensitivity of the material from the ultraviolet to the visible region, which is readily available from the sunlight on the earth, thus suggesting the great potential in solving ever-escalating global energy and environmental problems.[12] Up to now, many TiO_2 and doped-TiO_2 nanostructures, including nanofilms, hollow spheres, nanotubes, nanowires, and mesoporous structures, have been synthesized.[8,13−20] In particular, TiO_2 nanowires are often produced in nonaqueous media so that their anisotropic growth is kinetically favored. However, the ability to control the growth of TiO_2 nanowires is still rather limited in terms of nanowire quality and size, and the diameters of the nanowires that can be reliably synthesized are normally larger than 3 nm. Continuous shrinking of the TiO_2 nanowires to the angstrom-scale will require better molecular-level control. In this size regime reaching the atomic limit of 1D systems, quantum and surface effects are expected to be most pronounced, accompanied by dramatic changes in electronic structures and thus in the physical and chemical properties of the wires, which are anticipated to inspire new fundamental and technological research.

*Address correspondence to chsyang@ust.hk.

Received for review February 16, 2009 and accepted March 16, 2009.

Published online March 23, 2009.
10.1021/nn900157r CCC: $40.75

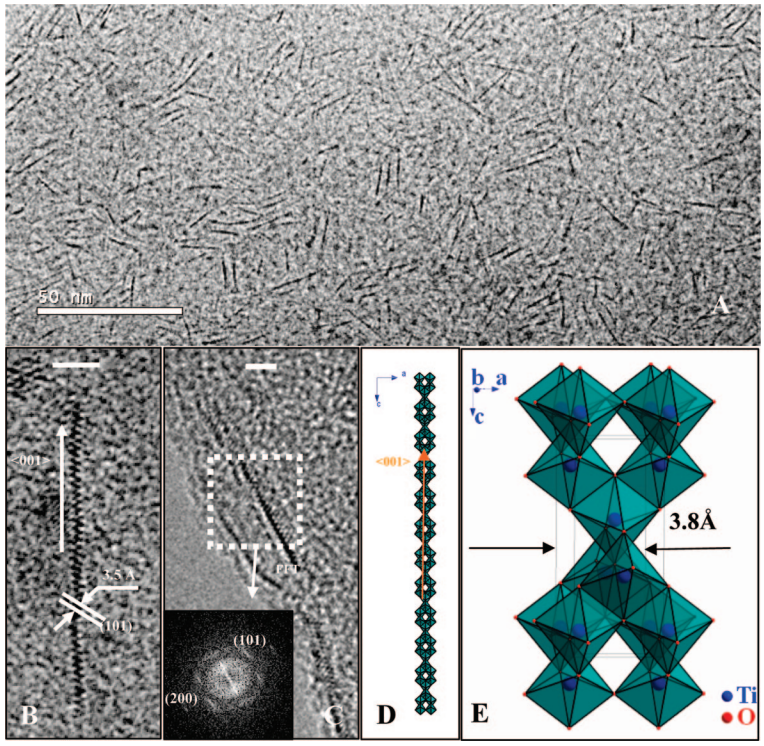

Figure 1. TEM micrographs of TiO_2 atomic wires. (A) Overview TEM images of nearly monodispersed atomic wires. (B) HRTEM image of a single atomic wire with a diameter of around 4.3 Å and lattice fringes spaced at about 3.5 Å intervals, corresponding to the spacing between the (101) planes of anatase TiO_2. The anatase atomic wire is along the direction of ⟨001⟩. (C) HRTEM image of atomic wires with the corresponding FFT pattern in the inset. (D) Model structure of an anatase atomic wire (viewed from *b* axis) growing along ⟨001⟩ direction. (E) Enlarged view of the 1D anatase structure in (D) with a single unit cell of anatase. Scale bar in B and C: 2 nm.

There has been considerable interest in the past few years in the fabrication of ultrathin nanowires of metals and semiconductors. For example, some isolated metal atom chains (Au, Mo) were fabricated by scanning tunneling microscopy and/or hard templates such as carbon nanotubes.[21,22] In addition, ultrathin crystalline CdSe nanoribbons (~1.5 nm)[23] and gold nanowires (~1.6 nm) were synthesized very recently by simple solution methods.[24] In the present work, we have reached the angstrom-scale dimension of the anatase TiO_2 wires by a scalable chemical solution method.

RESULTS AND DISCUSSION

Unlike most previous syntheses of TiO_2 nanowires, our method for the preparation of TiO_2 atomic wires is divided into two steps: the formation of the precursor and the growth of the atomic wires in the presence of surfactants. Although the two steps could be combined, we found that the two-step method worked much better as far as the product yield and quality are concerned. In addition, the reaction temperatures are relatively low for the synthesis of the atomic wires. These considerations above are all intended to prevent the rapid and thus noncontrollable growth of the TiO_2 phase so that the growth could be halted at the angstrom scale with the assistance of the surfactants.

We collected the reaction product in a deep yellow powder, but it could be easily redispersed in solvents such as hexane and chloroform without any irreversible aggregation. We used transmission electron microscopy (TEM, JEOL 2010 or JEOL 2010F, with an accelerating voltage of 200 kV) to examine the morphology of the reaction product at different levels of magnification. As shown in Figure 1A, the product almost exclusively consists of abundant, well-separated atomic wires with lengths of 10 to 25 nm, with an average of ~17 nm, and diameters uniformly smaller than 6 Å, typically ~4−5 Å (more detailed information on the size and size distribution measurements is shown in Figure S1, Supporting Information). The excellent dispersion of the atomic wires on the copper grid that was free of aggregation and bundling can be attributed to the protective surface layer of oleic acid. A survey of several atomic wires in a higher magnification TEM image (Figure 1B,C) further confirmed that the diameters of these atomic wires are indeed in the range of 4−5 Å, with an average of ~4.5 Å.

High-resolution transmission electron microscopy (HRTEM) images of two single atomic wires shown in Figure 1B,C provide additional and more detailed structural information. First and foremost, the atomic wires are clearly crystalline with well-defined lattice fringes that are spaced at about 0.35 nm intervals (as demarcated in Figure 1B), corresponding to the spacing between the (101) planes of anatase TiO_2. Figure 1B also reveals that these atomic wires grow along the ⟨001⟩ direction of anatase TiO_2, analogous to the anatase TiO_2 nanorods described previously with much larger diameters (>3 nm).[14−16] The inset of Figure 1C is a fast Fourier transform (FFT) pattern derived from the atomic wire image in the figure, which shows the presence of (101) spots in support of the structural analysis above. Schematically shown in Figure 1D,E is such an anatase atomic wire structure of TiO_2 viewed along the *b* axis. It is noticed that most of the atomic wires are quite straight within the 20 nm length scale owing to the good crystallinity with few defects, while some of the atomic wires show a certain degree of bending, which may be caused by imperfections in the anatase wire crystals as well as the surfactant monolayer assembly on the wire surfaces.

Because the atomic wires are so thin, X-ray powder diffraction gave only a weak broad bump at the location of the (101) reflection (Figure S2, Supporting Information). Nevertheless, as described below, X-ray photoelectron spectroscopy (XPS) and Raman scattering spectroscopy provided valuable information about the

composition and structure of the anatase TiO_2 atomic wires.

To ascertain the composition of the anatase atomic wires, we relied on XPS. The XPS survey spectrum of the atomic wires in a broad binding energy range is shown in Figure 2A, together with the estimated atomic concentrations. The atomic ratio of Ti/O is estimated to be about 1:3; the extra oxygen atoms can be ascribed to contributions from the capping layer of oleic acid. The high atomic concentration of C is evidence that the atomic wires are capped by oleic acid and/or oleylamine. Surprisingly, the atomic concentration of N is as high as 1.89%, which is much higher than the environmental contamination level (usually less than 0.1%) and hence indicates N-doping on the surfaces of the anatase atomic wires. More closely examined are four regions of the XPS spectrum, namely, the N 1s around 400 eV, the Ti 2p near 460 eV, the O 1s around 530 eV (Figure S3A, Supporting Information) and the C 1s near 285 eV (Figure S3B, Supporting Information). In Figure 2B, the relatively high intensity of the N 1s peak demonstrates the existence of N as a surface dopant in the atomic wires. Furthermore, the N 1s peak of nitrogen-doped TiO_2 atomic wires is centered at ~401 eV, which is notably higher than that in TiN crystals with a typical N 1s binding energy of ~397 eV. However, when the nitrogen atoms in TiN are partially replaced or oxidized by O atoms to form a sort of O−Ti−N or O−Ti−O−N structure on the atomic wire surfaces, the electron density around N is reduced due to the strong electron-withdrawing ability of the O atoms, leading to an increased N 1s binding energy.[25−27] Therefore, the relatively high N 1s binding energy we observed suggests that the N-doping of the TiO_2 atomic wires may well take the structural form of O−Ti−N or O−Ti−O−N−C on the atomic wire surfaces. To discern whether the N 1s peak is from the free oleylamine used as a reagent in the synthesis, we performed XPS spectroscopy on 1-hexadecylamine (HDA) in the N 1s core level region (see Figure S4 in Supporting Information). HDA used in place of oleylamine is simply for the convenience of the XPS experiment since the former is a solid whereas the latter is a liquid; both nevertheless have the same $-NH_2$ functional group. We found that the N 1s peak of HDA at ~399.4 eV is much lower in energy than that of the atomic wires at ~401.0 eV. This shows that the chemical state of the N atom in the alkylamine is very different from that in the atomic wires, and the latter appears to have a much lower electron density on the N atom. Clearly, the N 1s signal of the TiO_2 atomic wires is not from amine side chains that might be stuck onto the central TiO_2 core or from residual alkylamines that were not washed away completely, but rather from N-containing species as surface dopant of the atomic wires.

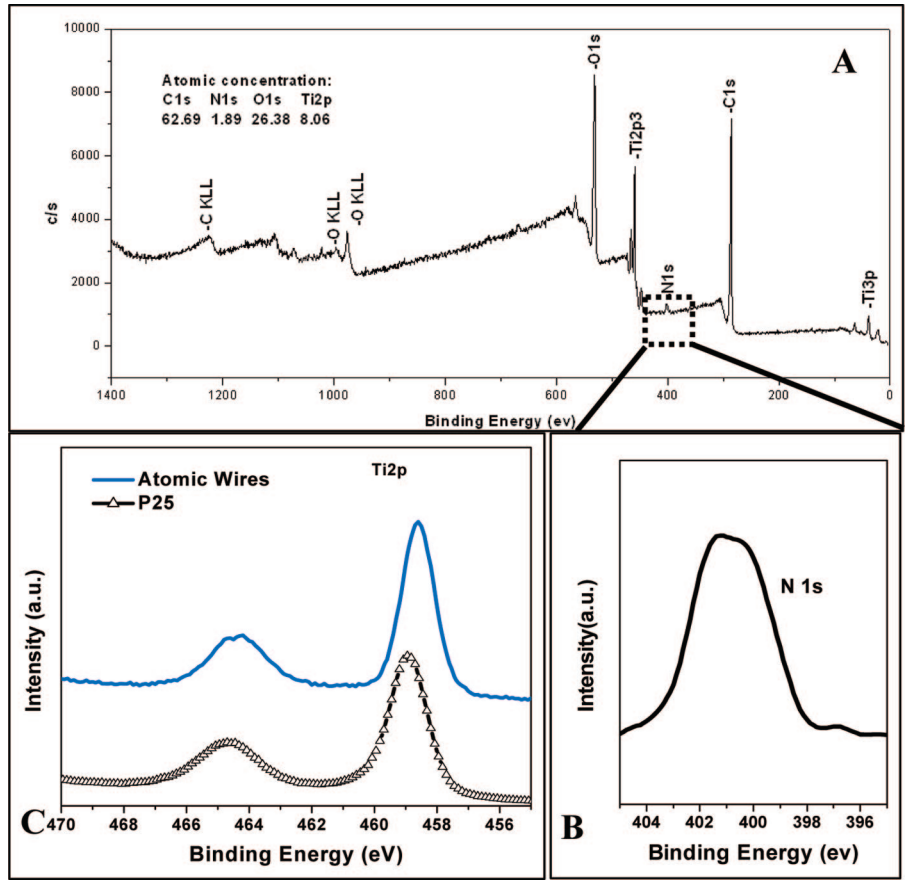

Figure 2. XPS spectra of the TiO_2 atomic wires. (A) XPS survey spectrum of the atomic wires in a broad binding energy range. A N 1s peak at around 401 eV is clearly seen in the spectrum. (B) Enlarged N 1s spectrum corresponding to the area in the marked square in (A). (C) Comparison of Ti 2p XPS spectra of the N-doped TiO_2 atomic wires and the P25 TiO_2 nanoparticles.

The Ti 2p spectrum shown in Figure 2C confirms that the oxidation state of titanium in the atomic wires is mainly +4, given that the peaks centered at 458.6 eV (Ti $2p_{3/2}$) and 464.3 eV (Ti $2p_{1/2}$) are similar to those of fully oxidized TiO_2. It is noteworthy that the Ti $2p_{3/2}$ peak at 458.6 eV for nitrided atomic wires is smaller by 0.3 eV than that for commercial P25 TiO_2 nanoparticles (Figure 2C) with a mean diameter of ~20 nm (see Figure S5, Supporting Information). Two explanations are possible in explaining the N-induced Ti 2p binding energy shift. First, the P25 TiO_2 nanoparticles may have a highly strained Ti^{4+} environment, and the incorporation of a nitrogen species may relieve the strain.[26] Second, the

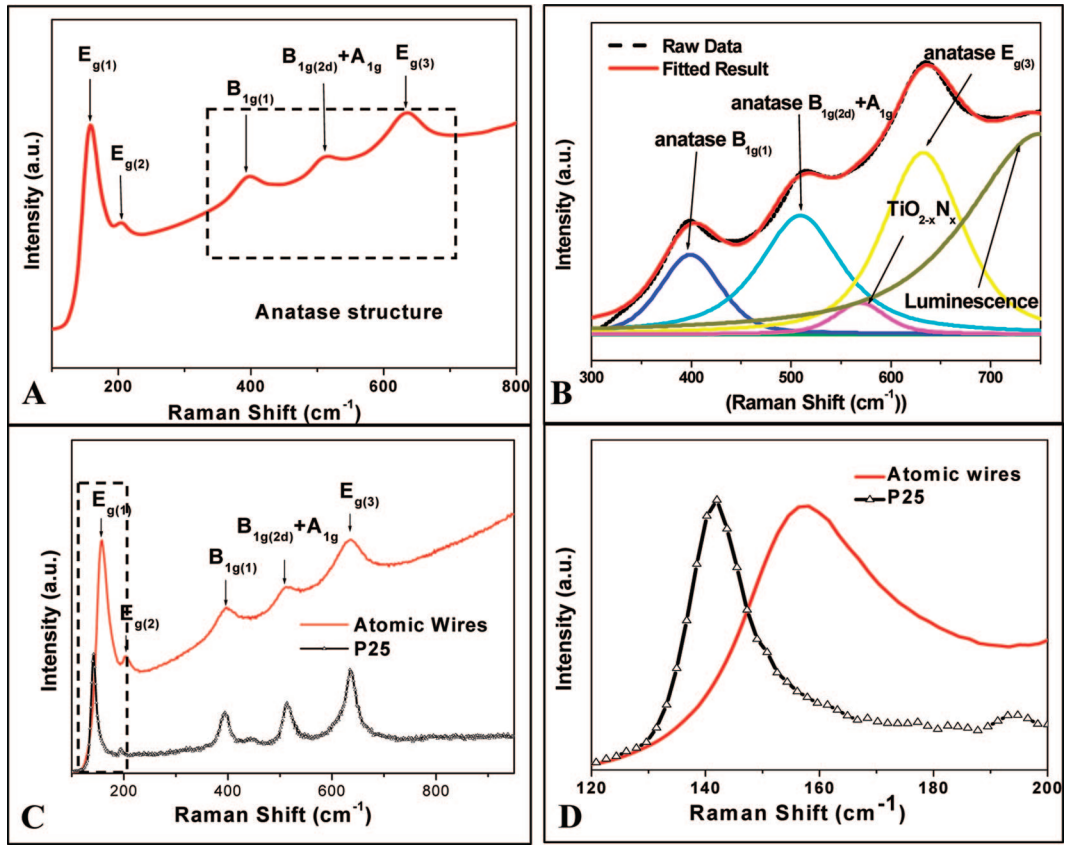

Figure 3. Raman spectra of the TiO_2 atomic wires. (A) Overall Raman spectrum of the TiO_2 atomic wires, in which the typical Raman peaks at around 158, 203, 404, 512, and 633 cm^{-1} can all be assigned to those of anatase TiO_2. (B) Enlarged Raman spectrum in the square area marked in (A). Besides the three fitted peaks, which can be attributed to the anatase TiO_2, an additional feature arises near 560 cm^{-1} (magenta color), which is identified as from the titanium oxynitride structure. (C) Comparison of Raman spectra of the N-doped TiO_2 atomic wires (red) and the P25 TiO_2 nanoparticles (black). (D) Enlarged Raman spectrum in the square area marked in (C).

substitution of nitrogen for oxygen could change the valence state of Ti^{4+} to Ti^{3+}, which would also lower the binding energy of the Ti $2p_{3/2}$ peak.[27] Spectra of O 1s and C 1s were also measured and analyzed (see Figure S3, Supporting Information), and the results further establish that the atomic wires are composed of TiO_2 surface doped with nitrogen.

More definite evidence of the structural phase of the TiO_2 atomic wires is provided by Raman spectroscopy. Shown in Figure 3A is a Raman spectrum of TiO_2 atomic wires. In general, the Raman peaks around 158, 203, 404, 512, and 633 cm^{-1} as well as the spectral pattern match well with the results reported in the literature for typical anatase TiO_2 nanocrystals. This represents an unambiguous proof of the anatase phase of TiO_2 atomic wires, which is difficult to obtain by other means such as XRD because of their extremely small size. More important, the fitting using the Peakfit software of the enlarged spectral portion shown in Figure 3B reveals an additional feature near 560 cm^{-1}. This feature, which was previously identified by György *et al.*[28] and verified by Prokes *et al.*,[26] can be attributed to the first-order scattering of a nonstoichiometric nitrogen-doped anatase TiO_2 structure, in accord with the XPS results described above.

Another striking feature of the Raman spectrum of TiO_2 atomic wires is the peak shift and broadening compared to that of 20 nm TiO_2 nanoparticles as shown in Figure 3C,D. The most intense $E_{g(1)}$ peak of the atomic wires (158 cm^{-1}) shows the largest blue shift from that of the 20 nm nanoparticles (142 cm^{-1}), as can be seen from Figure 3D. On the other hand, the full width at half-maximum (fwhm) of the $E_{g(1)}$ peak of the atomic wires is about twice that of the 20 nm nanoparticles. Similar band broadening and shifts are observed in other Raman vibration modes (Figure 3C). Occasionally, red shift is also observed, such as the peak at ~500 cm^{-1} due to different dispersion and/or other characteristics of the modes. The remarkable broadening and shift of the Raman peaks of TiO_2 atomic wires can be interpreted as mainly originating from the confinement of the phonons in anatase atomic wires.[8,29] On the other hand, some other factors, such as nonstoichiometry, and/or internal stress/surface tension effects arising from the drastic dimensional reduction to atomic scale wires, may also play a role in the shift and broadening of the Raman peaks. Further work is certainly needed to understand the phonon scattering in anatase atomic wires in greater detail. Also noteworthy is the presence of a strong luminescence background, which must be

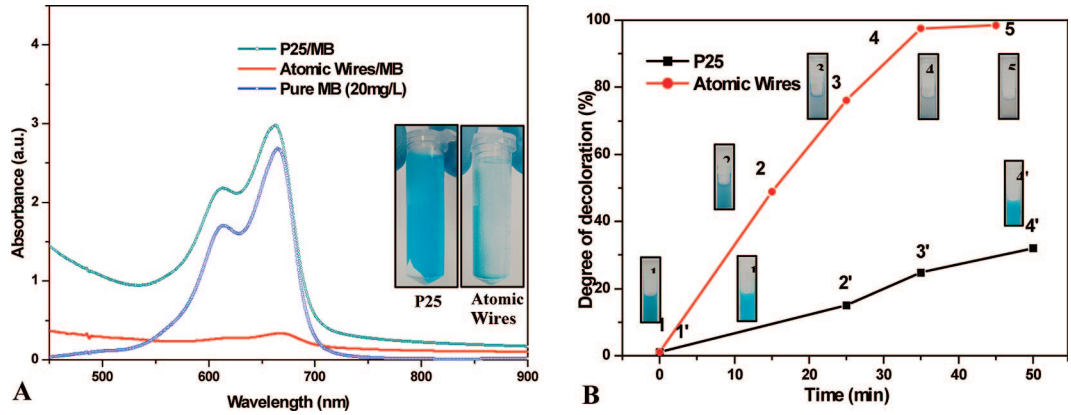

Figure 4. (A) UV−vis absorption spectra of pure MB solution (20 mg/L) (blue curve), 2 mL of the MB solution loaded with 8 mg of P25 nanoparticles after ultrasound-assisted adsorption for 1 h followed by centrifugation (dark cyan curve), and 2 mL of the MB solution loaded with ~4 mg of atomic wires after ultrasound-assisted adsorption for 10 min followed by centrifugation (red curve). The inset shows photographs of the MB/TiO_2 solutions after the ultrasonication and the subsequent centrifugation. (B) Photodegradation-induced decoloration rate of the atomic wires (red line) and P25 nanoparticles (black line). Photographs of the MB/TiO_2 solutions are given for the corresponding data points for directly viewing the visible-light-induced decoloration.

included in the fitting. Such visible-light-induced luminescence from the TiO_2 atomic wires is a consequence of the N-doping effect as observed previously in other material forms of anatase TiO_2.[26]

To answer the question about how thin a nanowire can be and stably exist in the ambient environment, we need consider both thermodynamic and kinetic factors in the formation of extremely thin nanowires (*e.g.*, atomic wires). Thermodynamically, the stabilization of the atomic wires is largely provided by carboxylic capping of atomic wires with oleic acid with the assistance of oleylamine. On the other hand, the long carbon chain of oleic acid prevents close approaches of atomic wires and renders the atomic wires kinetically stable. The key appears to be the tuning of the clustering reaction rates and surface capping, which favor the formation of atomic wires instead of overgrowth. In our two-step synthesis, the first step prepares the precursors, probably consisting of monomers and/or oligomers of TiO_x units, by esterification and ester elimination, and the second step leads to the coalescence of the monomers and oligomers and subsequent crystallization. The second step can be likened to the usual nucleation and growth of crystals. In forming atomic wires here, this step may proceed in a choked manner to restrict lateral overgrowth.

A direct revelation of the photocatalytic activity of the N-doped TiO_2 atomic wires can be attained by using a model reaction, *viz.*, photodegradation of methylene blue (MB) under visible light.[8,17,18,30] For this experiment, 4 mg of atomic wires was added into a 2 mL centrifuge tube filled with MB solution in DI water (20 mg/L). After ultrasonication in the dark for less than 10 min immediately followed by centrifugation, the solution turned clear and almost colorless while the atomic wires were precipitated with a blue color (inset of Figure 4A). This remarkable adsorbing ability owes to the exceptionally large surface-to-volume ratio of the atomic wires. In a control experiment to confirm the large specific surface area of the atomic wires, 8 mg of P25 nanoparticles of TiO_2 was used to supplant the atomic wires under otherwise the same conditions. No obvious decoloration could be observed even after over 1 h of ultrasonication (inset of Figure 4A). The corresponding UV−vis spectra in Figure 4A provide quantitative evidence that the atomic wires have adsorbed ~90% of the MB in the solution, whereas the absorption of MB on the P25 nanoparticle becomes almost negligible.

The MB-adsorbed atomic wire solution was subjected to photocatalytic degradation under irradiation of visible light ($\lambda \geq 400$ nm). By monitoring the visible adsorption peak of MB as a function of irradiation time (see Figure S6 in Supporting Information), we could estimate the rate of decoloration as shown in Figure 4B. The photographs corresponding to the data points provide a visual perception of the decoloration rate. It is seen that the degree of decoloration reaches almost 100% in <35 min. For the sake of comparison, the relevant decoloration data for the P25 nanoparticles of TiO_2 are also shown in Figure 4B. Evidently, the atomic wires display a much higher photocatalytic activity than that of the P25 nanoparticles. To test the recyclability, the used atomic wires were recentrifuged out from the decolorated solution, which became light grayish yellow after MB degradation (Figure S7A, Supporting Information). Despite losses of the atomic wire materials during the dispersion, test, and centrifugation procedures, we obtained a sufficient amount of the powder of about 1 mg. This recovered powder was still capable of adsorbing and photodegrading MB under visible light irradiation (Figure S7B−E, Supporting Information), manifesting that the atomic wire photocatalyst can be reused.

CONCLUSIONS

In this work, we have shown that atomic wires can indeed be stabilized and dispersed with appropriate surfactants in a solution setting by the bulk synthesis of prototypical TiO_2 atomic wires (~4−5 Å) with good anatase crystallinity. Crucial to the present work is to control the rates of precursor formation as well as the succeeding growth of the TiO_2 atomic wires in the presence of surfactants. In these extremely thin atomic wires, most of the atoms are on the surfaces and we have probably reached the small wire diameter limit, below which the concept of crystallinity does not apply anymore. The atomic wires are soluble and easily processable, and their synthesis is simple and scalable. This opens the way to access new material dimensions at the angstrom scale, which is anticipated to exhibit novel properties. Aside from being a new platform for fundamental research, these new materials are anticipated to serve as true 1D building blocks to construct new functional devices. Indeed, interesting size effects on phonon scattering of the TiO_2 atomic wires have already been observed, and preliminary photocatalytic degradation of methylene blue under visible light irradiation has been demonstrated.

METHODS

Synthesis of TiO_2 Anatase Atomic Wires. Appropriate amounts of oleic acid (OA, pract. 95%, International Laboratory USA, 3 mL) and cyclohexane (Acros, for analysis, 10 mL) were mixed. Into the mixture solution was slowly added dropwise $Ti(OBu)_4$ (Alfa Aesar, 98%, 0.5 mL). The resulting solution was sealed in a Teflon-lined stainless autoclave, heated to 150 °C, and kept for 25 h, and a wine red precursor solution was obtained. The sticky titanium precursor (viscous but transparent) was then extracted by precipitation with an excess of ethanol at room temperature, and a yellow powder was then collected.

The titanium complex precursor was redispersed in a mixture consisting of 5 mL of octadecene (ODE), 0.6 mL of OA, and 0.8 mL of oleylamine (OLA, Aldrich, tech, 70%). The solution was heated to and maintained at 180 °C in a three-neck flask with stirring for 1 h. The mixture appeared to be clear and light yellow, and then it turned dark yellow as the reaction proceeded, which indicated the formation of nitrogen-doped TiO_2 products.

Subsequent product extraction was performed in air at room temperature. Upon adding an excess of ethanol to the reaction mixture, the atomic wire product was precipitated. The precipitate was further purified by centrifugation and washed twice with ethanol to remove residual surfactants. The final N-doped TiO_2 atomic wires protected by OA coordination were easily redispersed in solvents, such as chloroform or hexane, without any sign of further growth or irreversible aggregation.

Characterization. The as-prepared products were characterized by transmission electron microscopy (TEM) and high-resolution TEM (HRTEM) using JEOL 2010 and JEOL 2010F microscopes with an accelerating voltage of 200 kV. Samples for TEM measurements were prepared by sonicating the precipitate products in hexane for 30 min and evaporating a drop of the suspension onto a carbon-coated, holey film supported on a copper grid. The XPS spectra were measured on a Perkin-Elmer model PHI 5600 XPS system with a resolution of 0.3−0.5 eV from a monochromated aluminum anode X-ray source with Kα radiation (1486.6 eV). The samples were powder dispersed on a carbon tape that was attached to the sample holder. The binding energies of the Ti 2p, O 1s, C 1s, and N 1s peaks from the samples were calibrated, with respect to the C 1s peak from the carbon tape at 285 eV. Raman spectroscopy was performed at room temperature in a Renishaw RM 3000 Micro-Raman system (spectral resolution $<1\ cm^{-1}$), employing an Ar^+ laser for excitation ($\lambda = 514$ nm) at a power of ~25 mW.

Photocatalysis Measurements. For photocatalytic degradation experiments, a methylene blue (MB) solution in distilled water was prepared with a concentration of 20 mg/L. To 2 mL of the MB solution in a centrifuge tube was added 4 mg of atomic wires. The mixture was ultrasonicated in the dark until the atomic wires were completely dispersed to form a uniform suspension. To estimate the degree of MB adsorption, the suspension was centrifuged at 2500 rpm for 20 min. In addition, a reference sample was prepared by dispersing 8 mg of P25 nanoparticles into 2 mL of the MB solution in a centrifuge tube, followed by ultrasonication and centrifugation.

The ultrasound-dispersed suspensions were loaded into quartz cuvettes (1 cm × 1 cm × 4 cm) and were exposed to the same simulated light source as used above except for additional filtering with a UV-cutoff filter (Andover Corporation 400FH90-25). Because the MB was completely adsorbed onto the atomic wires in less than 10 min of ultrasonication, the degree of decoloration due to photodegradation was estimated by monitoring the UV−vis absorption of the diluted suspension instead of the MB solution after centrifugation. After a given period of visible light irradiation, 100 μL of the MB/atomic wires suspension was pipetted into another cuvette and quickly diluted with distilled water to 2 mL for UV−vis absorption analysis. On the other hand, there was little adsorption of MB onto the P25 nanoparticles, hence UV−vis absorption of the supernatant after centrifugation was used to estimate the degree of decoloration due to photodegradation of MB. After a given period of light irradiation, the whole MB/P25 nanoparticles suspension was transferred from the cuvette to a centrifuge tube and then centrifuged at 2500 rpm for 10 min. The supernatant was transferred into another cuvette for UV−vis absorption analysis.

UV−vis absorption spectra were measured on a MILTON ROY Spectronic 3000 Array instrument. A linear calibration curve for the MB concentrations was obtained by monitoring the peak intensity at $\lambda_{max} = 665$ nm for a series of standard solutions and fitted according to the Beer's law.[30] The degree of decoloration is expressed as $(I_0-I)/I_0$, where I_0 is the relative absorbance (after baseline subtraction) at $t = 0$, and I is the relative absorbance (after baseline subtraction) after a given period of visible light irradiation.

Acknowledgment. We thank Hui Sun, Hong Deng, Wei Chen, and Tze Kin Cheung for helpful discussions. This work is supported by HKUST (RPC06/07.SC03) and the Research Grants Council of Hong Kong (GRF604206).

Supporting Information Available: Details on diameter and length measurements of the TiO_2 atomic wires, XRD and more detailed XPS analyses of the TiO_2 nanostructures, additional photocatalysis data of the TiO_2 nanostructures. This material is available free of charge *via* the Internet at http://pubs.acs.org.

REFERENCES AND NOTES

1. Xia, Y.; Yang, P.; Sun, Y.; Wu, Y.; Mayers, B.; Gates, B.; Yin, Y.; Kim, F.; Yan, H. One-Dimensional Nanostructures: Synthesis, Characterization, and Applications. *Adv. Mater.* **2003**, *15*, 353–389.
2. Duan, X.; Huang, Y.; Cui, Y.; Wang, J.; Lieber, C. M. Indium Phosphide Nanowires as Building Blocks for Nanoscale Electronic and Optoelectronic Devices. *Nature* **2001**, *409*, 66–69.
3. Pan, Z. W.; Dai, Z. R.; Wang, Z. L. Nanobelts of Semiconducting Oxides. *Science* **2001**, *291*, 1947–1949.
4. Braun, J. H.; Baidins, A.; Marganski, R. E. TiO_2 Pigment Technology: A Review. *Prog. Org. Coat.* **1992**, *20*, 105–138.

5. Pfaff, G.; Reynders, P. Angle-Dependent Optical Effects Deriving from Submicron Structures of Films and Pigments. *Chem. Rev.* **1999**, *99*, 1963–1982.
6. Fujishima, A.; Honda, K. Electrochemical Photolysis of Water at a Semiconductor Electrode. *Nature* **1972**, *238*, 37–38.
7. Hoffmann, M. R.; Martin, S. T.; Choi, W.; Bahnemann, D. W. Environmental Applications of Semiconductor Photocatalysis. *Chem. Rev.* **1995**, *95*, 69–96.
8. Chen, X.; Mao, S. S. Titanium Dioxide Nanomaterials: Synthesis, Properties, Modifications, and Applications. *Chem. Rev.* **2007**, *107*, 2891–2959.
9. Varghese, O. K.; Gong, D.; Paulose, M.; Ong, K. G.; Grimes, C. A. Hydrogen Sensing using Titania Nanotubes. *Sens. Actuators, B* **2003**, *93*, 338–344.
10. Grätzel, M. Photoelectrochemical Cells. *Nature* **2001**, *414*, 338–344.
11. Mor, G. K.; Shankar, K.; Paulose, M.; Varghese, O. K.; Grimes, C. A. Enhanced Photocleavage of Water Using Titania Nanotube Arrays. *Nano Lett.* **2005**, *5*, 191–195.
12. Livraghi, S.; Paganini, M. C.; Giamello, E.; Selloni, A.; Valentin, C. D.; Pacchioni, G. Origin of Photoactivity of Nitrogen-Doped Titanium Dioxide under Visible Light. *J. Am. Chem. Soc.* **2006**, *128*, 15666–15671.
13. Li, X.-L.; Peng, Q.; Yi, J-X.; Wang, X.; Li, Y. Near Monodisperse TiO_2 Nanoparticles and Nanorods. *Chem.—Eur. J.* **2006**, *12*, 2383–2391.
14. Cozzoli, P. D.; Kornowski, A.; Weller, H. Low-Temperature Synthesis of Soluble and Processable Organic-Capped Anatase TiO_2 Nanorods. *J. Am. Chem. Soc.* **2003**, *125*, 14539–14548.
15. Zhang, Z.; Zhong, X.; Liu, S.; Li, D.; Han, M. Aminolysis Route to Monodisperse Titania Nanorods with Tunable Aspect Ratio. *Angew. Chem., Int. Ed.* **2005**, *44*, 3466–3470.
16. Jun, Y.-W.; Lee, J.-H.; Choi, J.-S.; Cheon, J. Symmetry-Controlled Colloidal Nanocrystals: Nonhydrolytic Chemical Synthesis and Shape Determining Parameters. *J. Phys. Chem. B* **2005**, *109*, 14795–14806.
17. Asahi, R.; Morikawa, T.; Ohwaki, T.; Aoki, K.; Taga, Y. Visible-Light Photocatalysis in Nitrogen-Doped Titanium Oxides. *Science* **2001**, *293*, 269–271.
18. Sato, S. Photocatalysts Sensitive to Visible Light. *Science* **2002**, *295*, 626–627.
19. Burda, C.; Lou, Y.; Chen, X.; Samia, A. C. S.; Stout, J.; Gole, J. L. Enhanced Nitrogen Doping in TiO_2 Nanoparticles. *Nano Lett.* **2003**, *3*, 1049–1051.
20. Qiu, X.; Zhao, Y.; Burda, C. Synthesis and Characterization of Nitrogen-Doped Group IVB Visible-Light-Photoactive Metal Oxide Nanoparticles. *Adv. Mater.* **2007**, *19*, 3995–3999.
21. Nilius, N.; Wallis, T. M.; Ho, W. Development of One-Dimensional Band Structure in Artificial Gold Chains. *Science* **2002**, *297*, 1853–1856.
22. Muramatsu, H.; Hayashi, T.; Kim, Y. A.; Shimamoto, D.; Endo, M.; Terrones, M.; Dresselhaus, M. S. Synthesis and Isolation of Molybdenum Atomic Wires. *Nano Lett.* **2008**, *8*, 237–240.
23. Joo, J.; Son, J. S.; Kwon, S. G.; Yu, J. H.; Hyeon, T. Low-Temperature Solution-Phase Synthesis of Quantum Well Structured CdSe Nanoribbons. *J. Am. Chem. Soc.* **2006**, *128*, 5632–5633.
24. Huo, Z.; Tsung, C-K.; Huang, W.; Zhang, X.; Yang, P. Sub-Two Nanometer Single Crystal Au Nanowires. *Nano Lett.* **2008**, *8*, 2041–2044.
25. Chen, X.; Burda, C. Photoelectron Spectroscopic Investigation of Nitrogen-Doped Titania Nanoparticles. *J. Phys. Chem. B* **2004**, *108*, 15446–15449.
26. Prokes, S. M.; Gole, J. L.; Chen, X.; Burda, C.; Carlos, W. E. Defect-Related Optical Behavior in Surface-Modified TiO_2 Nanostructures. *Adv. Funct. Mater.* **2005**, *15*, 161–167.
27. Hashimoto, S.; Murata, A.; Sakurada, T.; Tanaka, A. Alternation of Ti 2p XPS Spectrum for TiO_2 by Ar Ion Bombardment. *J. Surf. Anal.* **2002**, *9*, 459–462.
28. György, E.; del Pino, A. P.; Serra, P.; Morenza, J. L. Surface Nitridation of Titanium by Pulsed Nd:YAG Laser Irradiation. *Appl. Surf. Sci.* **2002**, *186*, 130–134.
29. Choi, H. C.; Jung, Y. M.; Kim, S. B. Size Effects in the Raman Spectra of TiO_2 Nanoparticles. *Vib. Spectrosc.* **2005**, *37*, 33–38.
30. Konstantinou, I. K.; Albanis, T. A. TiO_2-Assistecd Photocatalytic Degradation of Azo Dyes in Aqueous Solution: Kinetic and Mechanistic Investigations: A Review. *Appl. Catal., B* **2004**, *49*, 1–14.